Universal rescaling of flow curves for yield-stress fluids close to jamming

M. Dinkgreve,[1] J. Paredes,[1] M. A. J. Michels,[2] and D. Bonn[1]
[1]*Van der Waals-Zeeman Institute, Institute of Physics, University of Amsterdam, Science Park 904, 1018 XH Amsterdam, The Netherlands*
[2]*Theory of Polymers and Soft Matter, Department of Applied Physics, Eindhoven University of Technology, P. O. Box 513, 5600 MB Eindhoven, The Netherlands*
(Received 1 April 2015; published 6 July 2015)

The experimental flow curves of four different yield-stress fluids with different interparticle interactions are studied near the jamming concentration. By appropriate scaling with the distance to jamming all rheology data can be collapsed onto master curves below and above jamming that meet in the shear-thinning regime and satisfy the Herschel-Bulkley and Cross equations, respectively. In spite of differing interactions in the different systems, master curves characterized by universal scaling exponents are found for the four systems. A two-state microscopic theory of heterogeneous dynamics is presented to rationalize the observed transition from Herschel-Bulkley to Cross behavior and to connect the rheological exponents to microscopic exponents for the divergence of the length and time scales of the heterogeneous dynamics. The experimental data and the microscopic theory are compared with much of the available literature data for yield-stress systems.

DOI: 10.1103/PhysRevE.92.012305 PACS number(s): 83.50.−v, 64.60.−i, 47.50.−d, 47.57.Bc

I. INTRODUCTION

Understanding and predicting the flow behavior of complex fluids is a subject of considerable industrial and fundamental interest [1]. Yield-stress fluids are an important class of complex fluids, and their flow behavior remains incompletely understood [2,3]. Most often, yield-stress fluids are a dispersion of one material in a continuous phase, e.g., suspensions of (soft) particles or polymers, foams, or emulsions. When sufficiently concentrated, these systems show a transition from mechanically solidlike to fluidlike states when the stress is increased above some critical value, the yield stress. The yield stress emerges in general when the volume fraction φ of the dispersed phase is higher than some critical value φ_c. This so-called jamming transition is currently a very popular subject in the fluid-dynamics and statistical-mechanics community and has received a lot of attention [4–12]. However it is not completely clear how generic the jamming description is, and whether, for instance, the mechanical behavior of jammed systems as a function of the volume fraction can be fully described or even predicted by considering the jamming transition to be analogous to an equilibrium critical phase transition [9,10,13–15]. The idea of jamming as a critical phenomenon, which is inspired by an observed power-law divergence of mechanical quantities with respect to the distance from the jamming transition, is what we will investigate here.

We first consider the relevant mechanical properties. For concentrated systems above the jamming transition, the flow behavior is often successfully described by the Herschel-Bulkley equation [16]

$$\sigma = \sigma_y + K\dot{\gamma}^{\beta} = \sigma_y[1 + (\tau_{\mathrm{HB}}\dot{\gamma})^{\beta}], \tag{1}$$

where σ is the shear stress, σ_y the yield stress, $\dot{\gamma}$ the shear rate, and K or τ_{HB} and β are adjustable parameters. One can then attempt to describe the vanishing of the yield stress with decreasing volume fraction as a power law in the distance to jamming:

$$\sigma_y = \sigma_0|\Delta\varphi|^{\Delta}, \tag{2}$$

with $|\Delta\varphi| = |\varphi - \varphi_c|$ and φ_c the "critical" (jamming) point. Below φ_c, the generically observed Newtonian-to-shear-thinning behavior with increasing shear rate can be well described by the Cross equation [17],

$$\sigma = \eta_N\dot{\gamma}/(1 + C\dot{\gamma}^{1-\delta}) = \eta_N\dot{\gamma}/[1 + (\tau_C\dot{\gamma})^{1-\delta}], \tag{3}$$

where C or τ_C and δ are again adjustable parameters; note that the shear-thinning regions of (1) and (3) are of the same form, with δ and C corresponding to β and η_N/K, respectively. The Newtonian viscosity η_N often satisfies a power law in $|\Delta\varphi|$, expressed by the Krieger-Dougherty equation [18],

$$\eta_N = \eta_0|\Delta\varphi|^{-M}, \quad \eta_0 = \eta_{\mathrm{sol}}\varphi_c^M; \tag{4}$$

η_{sol} is the viscosity of the continuous solvent phase.

The above equations, in particular some of the power laws in $\dot{\gamma}$ and $|\Delta\varphi|$, have been verified for many dissimilar systems, with often but not always similar values for each of the exponents β, Δ, δ, and M. For instance, the Herschel-Bulkley and Cross exponents β and δ are generally around 0.5 while for the yield-stress exponent Δ and the Krieger-Dougherty exponent M typically values between 1 and 3, and regularly close to 2, are reported (see Appendix C for a compilation of literature data with references).

Experimental and simulation studies report a power law similar to (2) also for the static shear modulus of the solidlike phase: $G = G_0|\Delta\varphi|^B$. With $\sigma_y = G\gamma_y$ this corresponds to a vanishing of the yield strain γ_y if $B < \Delta$, as sometimes reported (see, e.g., Ref. [19]), but B has also been found to have a similar value as Δ [20].

All the above equations apply to a steady state; however power-law scaling in time has also been reported for the transient creeping flow of a broad variety of dense complex systems close to their yield point but far from steady state. Independent of the stress, the instantaneous effective viscosity $\eta = \sigma/\dot{\gamma}$ and the cumulative strain $\gamma(t)$ often follow the so-called Andrade law [21],

$$\eta(t) \sim t^{\alpha}, \gamma(t) \sim t^{1-\alpha}, \tag{5}$$

over sometimes remarkably long times t. Such behavior was already observed by Andrade for metals in 1910 and has since

been reported, in the macroscopic rheology or in corresponding microscopic time scales, for, e.g., crystals [13,22–24], glasses [25], polymers [26], emulsions [27,28], gels [27,28], foams [27,28], sand [29], paper [30], and even complex biomaterials [31]. The value of the creep exponent α equally remarkably then often falls in a narrow interval 0.5–0.7.

Previously, some of us (see Paredes *et al.* [20]) have investigated the scaling in all the above equations on a single well-defined yield-stress system: a dense soft-sphere emulsion with supercritical and subcritical volume fractions φ, and established exponent values within the mentioned numerical ranges. Paredes *et al.* showed that by an appropriate scaling of the stress and rate with only two independent exponents all supercritical and subcritical flow curves could be mapped onto two master curves that merge at high shear rates. This was interpreted as evidence for a critical transition in the dynamics, from fluid to solidlike behavior. Collapse of supercritical Herschel-Bulkley data, with exponents very close to those of Ref. [20], had previously been reported by Nordstrom *et al.* for a different soft-colloid system [32]. Earlier, in two-dimensional (2D) simulations of overdamped soft disks, Olsson and Teitel reported a similar data collapse *and* a critical transition but with different power-law exponents [33]. Simulations by Otsuki and Hayakawa [34,35] for 2D, 3D, and 4D soft spheres with inertial dynamics gave qualitatively similar scaling, data collapse, and transition with density and could be rationalized with a similar scaling-ansatz approach; however, in this case the exponents and exponent relations proved independent of dimension and clearly differed from those in the experiments of Refs. [20] and [32] or those in the simulations of Ref. [33]. In equilibrium phase transitions, the exponents and exponent relations depend on dimensionality and symmetry, but not on details of the interactions. For jamming systems, some evidence of dimension-independent scaling, but with particle-interaction-dependent exponents differing from those in Ref. [20], has been given, e.g., in static simulations by O'Hern *et al.* [9,10] and/or in flow studies [36,37]. However, very recently Vågberg *et al.* [38] revisited this point and, based on two different simulation models, claim for their 2D case universal exponents in the flow of overdamped shear-driven frictionless systems.

The question is then whether the exponents that characterize the mechanical behavior depend on the (details of the) interparticle interactions. Paredes *et al.* propose that the critical transition happens because the mechanical behavior of systems near jamming is governed by a growing length scale associated with the heterogeneous dynamics, well above the length scale of the individual particles. In the loose analogy with equilibrium phase transitions one would then suppose that the exponent values are universal, i.e., independent of particle or interaction details. Heterogeneous microscopic dynamics is a frequently reported feature in various glassy or jamming systems investigated experimentally or by simulation, with a length scale of fluctuating cooperative motion well beyond the single-particle diameter, with a characteristic time scale of such fluctuations, and with accelerated particle motion under load [33,39–48]. Several studies report a divergence of such properties in approach of the yield stress, with power laws in stress, rate, or distance $|\Delta\varphi|$ [38,42,49–57]. These observations have suggested that, in spite of important differences [47,58–60], close analogies exist between glasses and jammed systems (see, e.g., Refs. [11,44]) and have given support to the idea [9,10,13–15] that the transition from flow to arrest in complex disordered systems under external load is a dynamic analog of thermodynamic second-order phase transitions, with analogous mesoscopic heterogeneity and power-law scaling, and that this transition is generic to a broad variety of such complex systems. Paredes *et al.* [20] outlined a simple microscopic two-state scaling theory that could rationalize the observed macroscopic flow and transition in terms of a critical divergence in the microscopic heterogeneous dynamics, with two independent microscopic scaling exponents only that agreed with their experiments.

The aim of the present paper is threefold. First, we seek more systematic order in the experimental results by comparing the flow behavior of a number of systems that are all 3D and overdamped but have different particle interactions. The focus is thereby mainly on the supercritical Herschel-Bulkley regime. Second, we elaborate in more detail the two-state microscopic model that was briefly outlined in Ref. [20]. Third, we compare the predictions of this model with our own experimental results and with a broad range of literature data, ordering the latter in comparable classes.

The paper is organized as follows. In the next section we experimentally investigate the steady-state rheology of different systems that exhibit a jamming transition. First, the difference between emulsions with mobile and rigid droplet surfaces is considered; second, the flow curves of two other complex liquids, a foam and a Carbopol gel, are examined. Scaling of the data onto master curves is investigated and the scaling exponents of the four systems are compared. In the following section the master-curve scaling and the critical transition from flow to jamming are described using a scaling ansatz, following [33]. To rationalize this scaling ansatz from a more microscopic point of view, we develop a model of the heterogeneous dynamics. The model results in a number of relations among the scaling exponents that can be verified experimentally. A comparison with our own flow-curve data and data from the literature is made in section four. We also briefly discuss creep measurements as an additional test to the model. In a final section conclusions are summarized, in particular on the microscopic origin of the observed scaling around the jamming transition and on the universality in this scaling among different systems. Three appendices discuss in more detail the mathematical derivation of the steady-state flow curve, the nature of the critical transition, and a broad range of literature data, respectively.

II. EXPERIMENTAL RHEOLOGY

A. Sample preparation

Two types of yield-stress emulsions have been prepared, one system with mobile particle surfaces and one with rigid surfaces. Rheological measurements have been performed using a controlled-shear-stress rheometer (CSS) (Anton Paar MCR 301) in a cone-plate geometry. Before carrying out the experiments samples were presheared at $100\,s^{-1}$ for 30 s and left to rest for another 30 s before the experiments started. Flow curves were obtained by performing an up-and-down shear-rate sweep.

The emulsions used are castor oil-in-water emulsions. In general, most types of surfactant-stabilized emulsions are considered as having mobile droplet surfaces and it is usually assumed that this leads to harmonic interactions between the drops [19]. Our mobile emulsions were stabilized using sodium dodecyl sulfate (SDS, from Sigma Aldrich), which is an ionic surfactant with molar formula $CH_3(CH_2)_{11}SO_4^-Na^+$. The rigid emulsions were stabilized using a protein solution composed of bovine serum albumin (BSA, from Sigma Aldrich) and a cosurfactant propylene glycerol alginate (PGA, from Dextra); this creates rigid surfaces on the droplets [61] and will thereby increase the drops' resistance to deformation. As a consequence, the mechanical properties of the system change and one would expect to see a difference in the flow curves.

Mobile castor oil-in-water emulsions were prepared in the following way:

(1) The continuous phase was prepared by dissolving SDS in ultrapure water (Milli-Q®), obtaining a solution with 1 wt% SDS concentration.

(2) The dispersed phase consisted of castor oil (Sigma-Aldrich).

(3) Emulsification: the oil was gradually added to the aqueous phase while stirring with a Silverson L5M-A emulsifier at 10 000 rpm for 2 min. During emulsification the sample was cooled in an ice bath to prevent heating of the sample. The internal volume fraction was $\varphi = 0.8$.

(4) Emulsions with lower φ were prepared by diluting the original emulsion ($\varphi = 0.80$) with the 1% SDS solution.

Rigid systems were prepared in a similar way, but with 0.4 wt% PGA and 0.4 wt% BSA instead of 1 wt% SDS in the continuous phase.

As a third system, SDS-stabilized foam was chosen. Data for this foam were obtained from previous research of S. Marze *et al.* [62], who studied the steady flow of three-dimensional aqueous foams at different volume fractions. The fourth system is a Carbopol "gel," for which different volume fractions were prepared as described in Ref. [63].

B. Rheology

1. Mobile emulsions

The results on the mobile emulsions were already reported in Ref. [20]. Flow curves were obtained by performing a shear-rate sweep as shown in Fig. 1(a). From these flow curves we determined that $\varphi_c \approx 0.645$; a linear extrapolation of the yield stress to zero gives $\varphi_c = 0.648 \pm 0.004$, whereas a quadratic fit works better and gives $\varphi_c = 0.645 \pm 0.005$. The curves above φ_c can each be fitted separately with the Herschel-Bulkley equation (1). However, the data for all these supercritical volume fractions can also be mapped onto one master curve by plotting $\sigma/|\Delta\varphi|^{\Delta}$ versus $\dot\gamma/|\Delta\varphi|^{\Gamma}$ and fitting $\Delta = 2.13$ and $\Gamma = 3.84$, see Fig. 1(b). Interestingly the flow data below φ_c then also collapse automatically onto a curve that coincides with the supercritical one at high rates. The supercritical master branch accurately follows the Herschel-Bulkley equation with $\beta = \Delta/\Gamma = 0.55$ and $K = 0.87$. The branch corresponding to fractions below φ_c can be fitted to the Cross equation (3) with $\delta = \beta$ and $C = \eta_N/K$, with the same values of β and K as above φ_c. The supercritical data can independently be scaled as σ/σ_y versus $\dot\gamma/\sigma_y^{1/\beta}$, giving a collapse with $\beta = 0.60$. All fitted parameters, including the prefactors σ_0 and η_0, are summarized with their uncertainties in Table I. Note that in Ref. [20] the Newtonian viscosity η_N was independently measured and found to accurately satisfy the Krieger-Dougherty equation (4), with an exponent fully consistent with the above exponent values, i.e., $M = \Gamma - \Delta = 1.71$ [see the inset of Fig. 1(b)]; the supercritical shear modulus G was found to vanish with $\Delta\varphi$ with the same exponent as the yield stress. These linear-response aspects will not be further discussed here, and we will focus on the flow curves.

2. Rigid emulsions

The flow curves obtained for the rigid emulsions are shown in Fig. 2(a). From these curves, using again a quadratic fit of the yield stresses versus $\Delta\varphi$ it is determined that $\varphi_c = 0.64 \pm 0.06$. All flow curves for supercritical volume fractions,

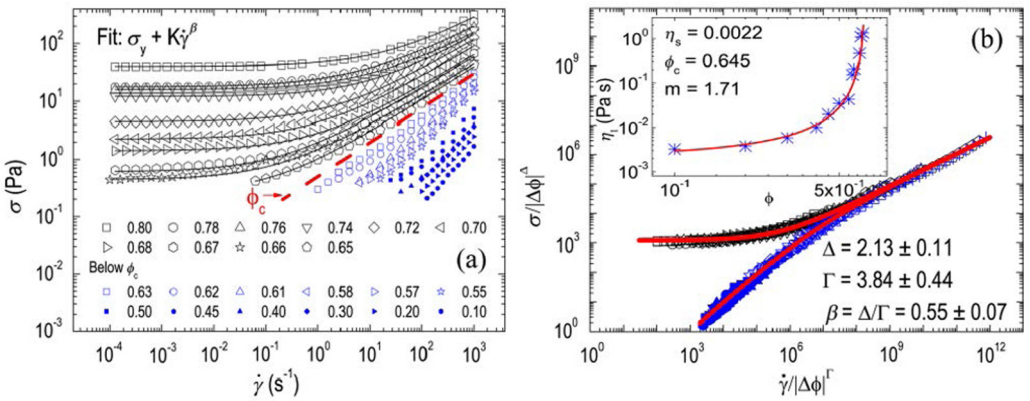

FIG. 1. (Color online) (a) Flow curves of mobile emulsions: Castor oil in water with 1 wt% SDS, for different internal volume fractions, showing Herschel-Bulkley fittings for $\varphi > \varphi_c$; symbols represent different volume fractions of the internal (oil) phase. (b) Master curve showing collapse of flow curves onto two branches, one for samples with $\varphi > \varphi_c$ and one for $\varphi < \varphi_c$, when plotted as $\sigma/|\Delta\varphi|^{\Delta}$ versus $\dot\gamma/|\Delta\varphi|^{\Gamma}$; the red lines are supercritical and subcritical branches representing the Herschel-Bulkley and the Cross fits of the master curve, respectively. Black symbols correspond to samples with $\varphi > \varphi_c$ and blue (gray) symbols correspond to samples with $\varphi < \varphi_c$; fit parameters are given in Table I. Inset in (b): Fit of the low-shear viscosity to the Krieger-Dougherty equation, giving $\eta_{sol} = 2.2\times10^{-3}$ Pa s and $M = 1.71$ with $\varphi_c = 0.645$ [20].

TABLE I. Overview of all rescaling parameters for the four systems: Mobile and rigid emulsions, foam, and Carbopol. The factor in the lowest row of the table is added as a numerical consistency check: The scaling approach to be discussed below shows that it should be of order unity.

Parameter	Mobile emulsion	Rigid emulsion	Foam	Carbopol
φ_c	0.645 ± 0.005	0.64 ± 0.06	0.68 ± 0.03	
Δ	2.13 ± 0.11	2.04 ± 0.13	2.21 ± 0.21	
Γ	3.84 ± 0.44	3.80 ± 0.34	3.75 ± 0.20	
$\beta = \Delta/\Gamma$	0.55 ± 0.07	0.54 ± 0.06	0.59 ± 0.07	
β (from σ_y scaling)	0.60 ± 0.08	0.54 ± 0.08	0.57 ± 0.09	0.48 ± 0.14 0.55 ± 0.04*
K	0.87	4.25 ± 0.39	2.53 ± 0.12	11.85 ± 0.11 11.77 ± 0.18*
σ_0(Pa)	1100	2315 ± 59	497 ± 10	
η_0 (Pa s)	0.001			
$\sigma_0^{1-\beta}\eta_0^{\beta}/K$	0.60			

*Leaving out the lowest concentration of 0.10 wt% (see text).

each obeying the Herschel-Bulkley equation, can be rescaled onto one master plot in the same manner as above, using $\Delta = 2.04$ and $\Gamma = 3.80$; these collapsed data fit to a Herschel-Bulkley equation with $\beta = \Delta/\Gamma = 0.54$ and $K = 4.25$. Once again, all flow data below φ_c then automatically also collapse with this procedure onto a single curve, which meets the supercritical one at high rate, Fig. 2(b). However, as is clear from the slopes in Fig. 2(a), all subcritical samples are still shear thinning even at the lowest rates. As a consequence, no reliable value for η_0 can be obtained from a master fit of the collapsed data to the Cross equation. Direct scaling of σ/σ_y versus $\dot{\gamma}/\sigma_y^{1/\beta}$ also gives $\beta = 0.54$. The final results are very similar to the rescaling found for the mobile emulsions, see Table I.

3. Foam

All flow curves as measured by Marze *et al.* [62] for different volume fractions were fitted with the Herschel-Bulkley equation, Fig. 3(a). The critical volume fraction was determined by a quadratic fit of the yield stresses, resulting in $\varphi_c = 0.68 \pm 0.03$; this value is somewhat higher than that of random close packing, which may be due to the larger size polydispersity. Once again, all flow curves can be rescaled and collapsed onto one master curve when plotted as $\sigma/|\Delta\varphi|^{\Delta}$ versus $\dot{\gamma}/|\Delta\Gamma|^{\Gamma}$, for $\Delta = 2.21$ and $\Gamma = 3.75$, Fig. 3(b). The Herschel-Bulkley representation of the latter gives $\beta = \Delta/\Gamma = 0.59$ and $K = 2.53$. Direct scaling of σ/σ_y versus $\dot{\gamma}/\sigma_y^{1/\beta}$ gives $\beta = 0.57$, see also Table I.

4. Carbopol

For the Carbopol gels with different volume fractions the flow curves were obtained by performing the same rheological procedure as for the yield-stress emulsions, Fig. 4(a). The considered weight fractions are very low, but due to the strong pH-dependent swelling of the spongelike particles a Herschel-Bulkley fit with a yield stress and shear thinning is showing up at all concentrations. It is hard to define a meaningful single critical volume fraction for these expanding gels, but the data for all volume fractions can still be collapsed onto one master curve by direct scaling with the yield stress, Fig. 4(b). The master curve fits the Herschel-Bulkley equation with $\beta = 0.48$ and $K = 11.85$. The relatively large error bound of about 30%

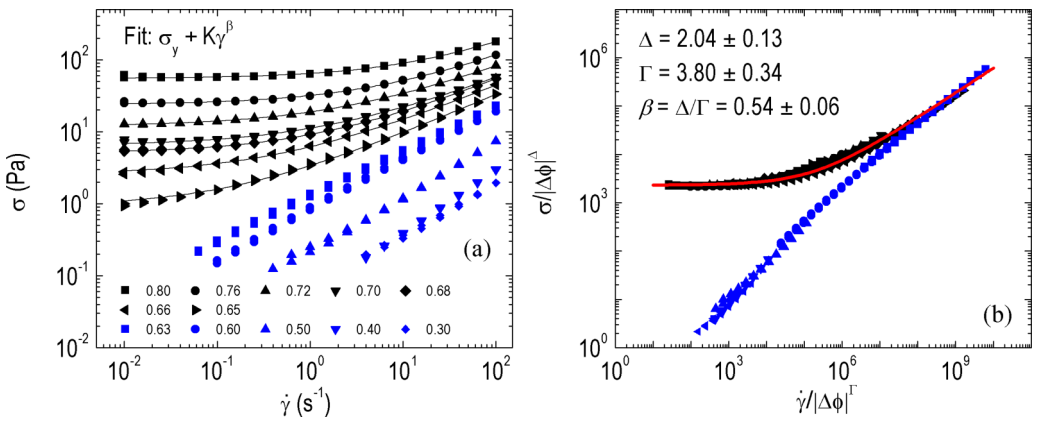

FIG. 2. (Color online) (a) Flow curves of rigid emulsions: Castor oil in water with 0.4 wt% BSA and 0.4 wt% PGA for different internal volume fractions. (b) Master curve showing collapse of flow curves onto two branches, one for samples with $\varphi > \varphi_c$ and one for $\varphi < \varphi_c$, when plotted as $\sigma/|\Delta\varphi|^{\Delta}$ versus $\dot{\gamma}/|\Delta\varphi|^{\Gamma}$; the red line is the supercritical branch representing the Herschel-Bulkley master fit. Black symbols correspond to samples with $\varphi > \varphi_c$ and blue (gray) symbols correspond to samples with $\varphi < \varphi_c$; fit parameters are given in Table I.

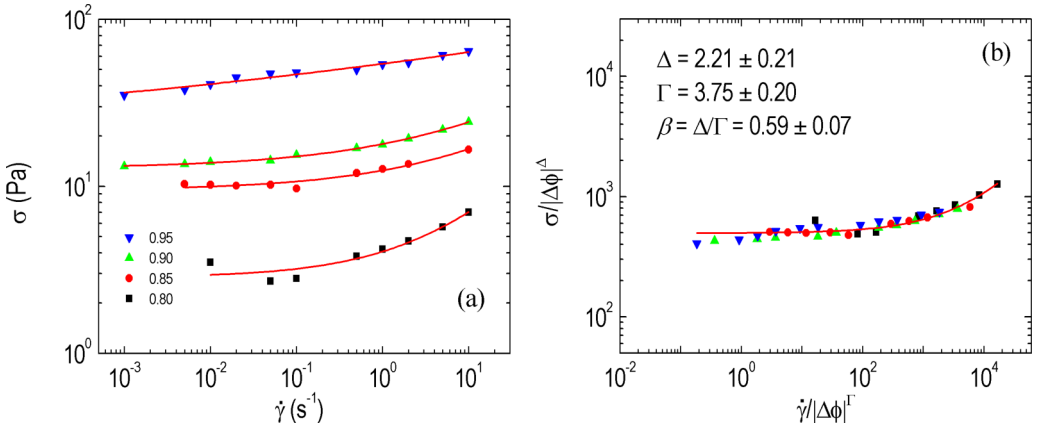

FIG. 3. (Color online) (a) Flow curves for SDS foams for different liquid volume fractions (experimental data from Ref. [62]). The red lines show Herschel-Bulkley fittings. (b) Master curve showing the collapse of flow curves onto one, when plotted as $\sigma/|\Delta\varphi|^{\Delta}$ versus $\dot{\gamma}/|\Delta\varphi|^{\Gamma}$. The different symbols represent different volume fractions; fit parameters are given in Table I.

in β is mainly due to the lowest concentration; if the data for this concentration are omitted a much better master fit follows, with $\beta = 0.55$ and $K = 11.77$, see also Table I.

C. Summary of the experimental data

Different systems were investigated and rescaled with simple power laws in the distance to jamming, giving supercritical and (where accessible) subcritical master curves. As indicated before by Paredes *et al.* [20], the combined Herschel-Bulkley and Cross equations nicely describe such flow behavior for a single simple yield-stress emulsion. We have shown here that these combined equations can be used to successfully describe the flow behavior near jamming for four different systems: mobile and rigid emulsions, foam, and Carbopol. All of the individual systems are rescaled onto one single master curve by plotting $\sigma/|\Delta\varphi|^{\Delta}$ versus $\dot{\gamma}/|\Delta\varphi|^{\Gamma}$, with fitting parameters as shown in Table I. As a remarkable result, all different systems can be rescaled with exponents that within numerical uncertainty have common values: $\Delta \approx 2.1$, $\Gamma \approx 3.8$, and $\beta = \Delta/\Gamma \approx 0.55$. This strongly supports the conclusion that the flow behavior of such overdamped yield-stress materials can be described by one universal scaling form, independent of the mechanical properties of the system. A similar claim was made recently by Vågberg *et al.* [38], based on two simulated 2D systems.

III. SCALING AND MICROSCOPIC MODEL

A. Scaling ansatz

The collapse of all rheological data on two master curves by the scaling of the two axes with the appropriate power laws in $|\Delta\varphi|$, as demonstrated in Figs. 1–4, leads to the assumption that the rheology above and below the jamming concentration has one common origin. Such a collapse was already shown for other soft-colloid dispersions [32] and also seen in simulations [33–35,64]. The assumption is mathematically expressed by a scaling ansatz [33] similar to the Widom scaling for equilibrium critical phase transitions:

$$\sigma = \sigma_0|\Delta\varphi|^{\Delta} F_{\pm}(\eta_N\dot{\gamma}/\sigma_y) = \sigma_0|\Delta\varphi|^{\Delta} F_{\pm}(\eta_0\dot{\gamma}/\sigma_0|\Delta\varphi|^{\Gamma}). \quad (6)$$

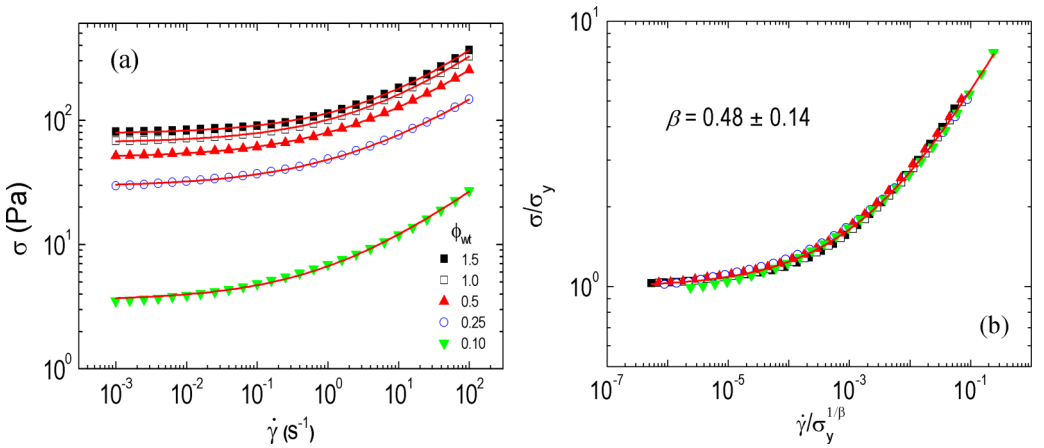

FIG. 4. (Color online) (a) Flow curves of Carbopol for different internal volume fractions. The red lines show the Herschel-Bulkley fittings. (b) Master curve showing collapse of all flow curves onto one, when plotted as σ/σ_y versus $\dot{\gamma}/\sigma_y^{1/\beta}$. The different symbols represent different volume fractions; fit parameters are given in Table I.

Here $F_{\pm}(z)$ is a crossover function that modifies the supercritical linear-elastic behavior depending on the ratio of viscous to elastic stresses, both for supercritical (+) and for subcritical (−) concentrations. So for $z \ll 1$ we must have $F_+(z) = 1$ and $F_-(z) = z$; for $z \gg 1$ we get $F_{\pm}(z) = Az^{\beta}$, with $\beta = \Delta/\Gamma$ to ensure that (6) is independent of concentration in the critical limit $\varphi = \varphi_c$; A is an unspecified constant of order unity. The equation for large z corresponds to the shear-thinning regime, since it implies $\sigma = A\sigma_0(\eta_0\dot{\gamma}/\sigma_0)^{\beta}$. It expresses that here the super- and subcritical systems become indistinguishable. This is obviously the case at the critical concentration, but as the argument of the crossover function shows the critical regime widens at high rate, with crossover rates for critical shear-thinning behavior at either side of φ_c satisfying (apart from a constant of order unity):

$$\dot{\gamma}_{\mathrm{co}} = (\sigma_0/\eta_0)|\Delta\varphi|^{\Gamma}. \tag{7}$$

Identifying the above results with the power laws in the empirical Herschel-Bulkley, Cross, and Krieger-Dougherty equations we have $\beta = \delta$, $K = \eta_N/C = A\sigma_0^{1-\beta}\eta_0^{\beta}$, $M = \Gamma - \Delta$. Note that apart from a constant of order unity the relaxation rates $1/\tau_{\mathrm{HB}}$ and $1/\tau_C$ of the Herschel-Bulkley and Cross equations equal the critical crossover rate (7). While the scaling ansatz is thus able to reproduce with only two independent scaling exponents the phenomenology of the observed rheology scaling across the critical concentration, both in the linear and shear-thinning regimes, a microscopic model is still needed to explain it.

B. Microscopic model

1. *Two-state heterogeneous dynamics*

Based on the experimentally observed scalings we now propose a simple model of microscopic heterogeneous dynamics to explain the macroscopic rheology around the critical concentration for jamming. As mentioned in the Introduction, the observed flow mechanics is common to many experimental and simulated systems for which such heterogeneous dynamics has been reported and has led to the suggestion that the underlying cause is a generic second-order critical transition in the dynamics, between a stagnant and a fluid phase. Here we follow this suggestion and attempt to explain the data from a simple and *ad hoc* two-state model for such a transition.

The power-law divergence of the Newtonian viscosity and the power-law vanishing of the shear modulus or yield stress are commonly understood from the existence of a diverging length scale ξ that characterizes correlated motion, i.e., the typical length over which particle displacements cannot be considered independent. In experiments [45,47,49–51,57] and simulations [33,53,54,65–69] such a divergent length scale has been observed both in the linear regime around φ_c and when approaching the yield-stress line of quasistatic flow at higher concentrations φ. Since under stresses above the yield stress the stagnant phase starts flowing, we assume that under stress a fraction s of the particles remains stagnant in neighbor cages while the fraction 1-s becomes fluidized. This simple two-state picture represents what are in reality two sides of a very broad mobility distribution. In view of the observations we make an analogy with the linear regime and assume that the length scale ξ of correlated, heterogeneous dynamics diverges when s approaches a critical value s_c where macroscopic flow halts; this critical fraction for jamming will be below unity. Following the idea that the divergence is similar to that near a second-order phase transition, we can subsequently choose the divergent length scale as the single dominant variable that governs macroscopic behavior. Mathematically this single relevant variable implies that ξ can only diverge as a power-law in the distance $\Delta s = |s - s_c|$ from critical jamming and that other variables in their dependence on s near s_c derive from ξ again as power laws, with similar critical behavior. In particular, this applies to the lifetime τ_{het} of the fluctuating heterogeneity pattern and to the average time τ_η for the single-particle mobility, i.e., the time for the average particle to move over a distance of its own diameter. The latter time scale τ_η is directly proportional to the average viscosity η of the system. So in fact $\xi(s), \tau_{\mathrm{het}}(s), \tau_\eta(s)$, and $\eta(s)$ are all interrelated by power laws in Δs. Normalizing them to their values at $s = 0$ and introducing critical exponents ν, m, and n we can then write:

$$\begin{aligned}\xi(s)/\xi_a &= [\tau_{\mathrm{het}}(s)/\tau_a]^{\nu/n} = [\tau_\eta(s)/\tau_a]^{\nu/m} \\ &= [\eta(s)/\eta_a]^{\nu/m} = |1 - s/s_c|^{-\nu}.\end{aligned} \tag{8}$$

The length scale ξ_a is of the order of the single-particle diameter. The limiting times $\tau_\eta(0)$ and $\tau_{\mathrm{het}}(0)$ will have a similar scale and have for simplicity been taken equal to a single time τ_a; however, for an increasing fraction s of stagnant particles the heterogeneity lifetime τ_{het} will become much larger than the fluidity time τ_η, so its associated exponent will be larger: $n > m$. Since the ratio $\tau_{\mathrm{het}}/\tau_\eta$ of the two microscopic time scales diverges near s_c we can interpret $\eta_a = \eta(s = 0)$ as the asymptotic viscosity of a fully fluidized phase and treat the arrested domains as a dispersed solid phase. Note that in this interpretation the last equality in (8) is a logical generalization of (4) if we choose the same exponent $m = M$ as in the Krieger-Dougherty equation. This supposes a deep relation between the linear and the nonlinear rheology, with the same physics in (4) and (8); indeed, a deep connection is already implied by the empirical collapse of data over the full dynamic range in Figs. 1–4, with a direct relation between the empirical exponents M, Γ, and Δ, viz. $M = \Gamma - \Delta$. We will return to this point later. Both τ_a and η_a will be continuous functions of φ near φ_c and in comparison with the functions that depend as a power law on $|\Delta\varphi|$ they may be treated as constants sufficiently close to φ_c; together they define a characteristic asymptotic high stress $\sigma_a = \eta_a/\tau_a$.

The internal parameter of our model, the stagnant fraction s, is determined by a competition between stress-induced escape of arrested particles from their cages, and fluctuation-induced arrest of mobile particles; the latter arrest mechanism will be dependent on this internal variable s and will be detailed later. The time evolution of the stagnant fraction $s(t)$ can then be given by a simple first-order kinetic equation:

$$ds/dt = -s/\tau_R + (1 - s)/\tau_A, \tag{9}$$

with $1/\tau_R$ the relaxation rate for the arrested particles to become mobile and $1/\tau_A$ the rate with which mobile particles become arrested again.

The relaxation rate $1/\tau_R$ can be considered as resulting from either of two typical mechanisms. For low stress we may consider that particles are caged by a large energy barrier ε and that the applied stress, thermal energy, or a combination of both facilitates barrier crossing of single particles; this process is characterized by a typical barrier stress σ_b. Subsequently, with increasing stress and hence increasing number of such crossings a collective flow process develops in which the cage itself vanishes; the latter process takes over when the average rate $\dot\gamma$ becomes of the order of the single-particle escape rate or larger. So in a simple approximation we can write:

$$1/\tau_R = (1/\tau_b) f(\sigma/\sigma_b) + \dot\gamma, \tag{10}$$

with τ_b the typical time for barrier crossing at stresses near σ_b; around the solid-fluid transition that we are interested in this time scale will be orders of magnitude larger than τ_a. In fact, the ratio τ_b/τ_a, still a function of φ, will be the dominant large parameter in the model and will be much larger than any dimensionless experimental time scale $(\tau_a \dot\gamma_{\rm exp})^{-1}$ in the limit $\varphi \uparrow \varphi_c$ and beyond.

For athermal jamming systems repulsive energies dominate over thermal energies, and the limit of zero temperature has to be assumed before applying shear [58–60]. The barrier stress σ_b is then a sharply defined yield stress $\sigma_y(\varphi)$ below which the deformation is elastic and no flow is possible; it scales as $\varepsilon/v_{\rm act}$, with $v_{\rm act}$ some local activation volume needed for a single relaxation event, and vanishes below the critical volume fraction φ_c. So above φ_c we can assume the simple form $f_+(x) = (x-1)^p$ for $x > 1$ and $f_+(x) = 0$ for $x < 1$, with some positive exponent p to be discussed later. Below φ_c we can take $f_-(x) = 1$ since at low stress the rheology should be Newtonian. Note that there is continuity in $f(x)$ across the jamming point φ_c along the line $x = 2$, i.e., $\Delta\sigma = \sigma_y$.

For high but finite ratios ε/k_BT thermal processes may at very large time scales still relax the elastic stress in the solid within experimental time scales. This intermediate case between glassy dynamics and jamming may be described by adding up the probabilities for stress-induced and thermally induced cage escape, i.e., adding to (10) the rate for thermal barrier crossing. That process is an Eyring-type cage escape [70], for which the characteristic time constant τ_b is the equilibrium α-relaxation time and the typical barrier stress σ_b is $k_BT/v_{\rm act}$. The stress dependence above φ_c is in the Eyring model given by $f_+(x) = x^{-1}\sinh x$; it crosses over from parabolic at low stress to exponential at high stress. This thermal scenario applies to glasses, i.e., when shear is applied before considering the limit of low temperatures [58–60,71,72]. Heterogeneous dynamics, accelerated dynamics in approach of the yield point, and subsequent flow of monomers has also been studied in polymer glasses, and the analogy with jamming has been noted [42,44,46,48]. An Eyring-type near-Gaussian decrease of the single-particle relaxation time with stress, as discussed around Eq. (10) is revealed in simulations [43]. In view of the nature of the systems that we studied experimentally we henceforth consider the athermal limit of frictionless repulsive particles only. Effects of particle friction and attraction will change the local dynamics and bulk rheology and have been studied, e.g., in Refs. [73,74].

With the expression (10) a deep connection is again assumed between the dynamics near equilibrium and far in the nonlinear regime. It is worthwhile noting that a similar expression was introduced to explain strain-rate – frequency superposition in the rheology of soft materials [75].

2. The steady state

The steady-state stagnant fraction s, and hence the viscosity (8), follows as a function of σ or $\dot\gamma$ by putting the left-hand side of (9) equal to zero, which gives the rate balance $s/\tau_R = (1-s)/\tau_A$; either of these terms may now be taken as the rate $1/\tau_{\rm het}$ with which the heterogeneity pattern fluctuates. So we get as the steady-state condition for s and η:

$$s[(\tau_a/\tau_b) f(\sigma/\sigma_y) + \tau_a\dot\gamma] = (1 - s/s_c)^n = (\eta_a/\eta)^{n/m}. \tag{11}$$

Solving this set of equations we can derive the flow curve of σ versus $\dot\gamma$, or, equivalently, the viscosity η versus σ, and simultaneously have insight in the underlying microscopic heterogeneity through the instantaneous stagnant fraction $s = s(\sigma)$. The mathematics is worked out in Appendix A. In the solution four different regimes of flow are recognized: (I) Newtonian flow at low rate in absence of a yield stress, so for subcritical concentrations; (II) a stress plateau ending in the yield stress at vanishing rate, so for supercritical concentrations; (III) power-law shear-thinning flow that makes the distinction between the two low-rate regimes (I) and (II) vanish at rates above $1/\tau_b$; and (IV) a second Newtonian regime above the very high relaxation rate $1/\tau_a$, for both concentration domains. The regimes I-III are easily identified as those seen in the experimental data of Figs. 1–4. The regime IV may well be inaccessible experimentally for many systems but is predicted by our model; it will not be discussed here further. For the regimes I–III the model predictions coincide with the empirical Herschel-Bulkley and Cross equations (1) and (3) when we make the identifications $\eta_N = \eta_a(\tau_b/\tau_a)^{m/n}$, $K = \eta_N/C = \eta_a/\tau_a^{m/n}$, and $\beta = \delta = 1 - m/n = 1/p$.

3. Recovering the scaling ansatz

The model describes the different regimes around the solid-fluid transition in a unified manner. It focuses on the dependence on flow rate $\dot\gamma$ and, via the stress- or rate-dependent order parameter s, on the relation with the heterogeneity in the microscopic kinetics; in particular, the power laws involving the exponents m and n relate to diverging microscopic time scales. So far, the mathematical solution makes no connection with the dependence on the concentration φ or with the empirical exponents Γ, Δ, and $M = \Gamma - \Delta$. This connection is now easily made by employing the assumed relation between the microscopic physics of the quasistatic and nonlinear regimes; the equations (4) and (8) for η, valid in these two regimes, respectively, both express the dependence of a fluid viscosity on solids content, so the exponents may be identified: $M = m$. From the result $\Delta/\Gamma = \beta = 1 - m/n$ we then immediately get $\Gamma = n$, $\Delta = n - m$. Having thus found the macroscopic exponents in terms of the microscopic ones we can also incorporate the φ depencence by equating the macroscopic crossover rate (9) to $1/\tau_b$, which gives $\tau_b = (\eta_0/\sigma_0)|\Delta\varphi|^{-n}$. Inserting this into the expression just found for η_N we recover the Krieger-Dougherty result (4), with the asymptotic high-rate

viscosity η_a now also related to the yield-stress prefactor σ_0 and to the solvent viscosity $\eta_{\rm sol} = \eta_0/\varphi_c^M$, i.e., to the parameters of the linear response: $\eta_a = \eta_0(\tau_a\sigma_0/\eta_0)^{m/n}$. Equation (2) for the dependence of the yield stress on φ is now automatically implied, since it was used to derive (9) and hence τ_b; the prefactor σ_0 in this equation cannot be detailed further since it relates to the elastic deformation, which is beyond the scope of the present paper. In summary, with all these identifications we have recovered the full scaling ansatz (6) from the microscopic model.

4. Heterogeneous dynamics around the critical transition

The development of the heterogeneous dynamics as a function of stress σ and concentration φ is recovered from the model by using the relation (8) of the microscopic order parameter s with the viscosity $\eta = \eta(\sigma,\varphi)$. In particular it gives in the low-rate Newtonian regime, and hence also at the crossover (co), a linear scaling of $|\Delta s|$ with $|\Delta\varphi|$:

$$|\Delta s/s_c| = |\Delta s_{\rm co}/s_c| = (\eta_0/\sigma_0\tau_a)^{-1/n}|\Delta\varphi|. \qquad (12)$$

This shows that our two-state model predicts even in the low-rate Newtonian regime a finite and increasing heterogeneity on approach of φ_c. In reality this discrete heterogeneity should be interpreted as a strong broadening of the continuous mobility distribution. Similarly, the heterogeneity length scale ξ and time scale $\tau_{\rm het}$ follow from the solution of $\eta(\sigma,\varphi)$ by using (8). In particular, at the critical concentration, and by extension also in the regime of critical shear thinning, they are found to diverge in a power-law fashion for vanishing stress or rate:

$$\xi/\xi_a = (\tau_{\rm het}/\tau_a)^{\nu/n} = (\eta_a/\tau_a\sigma)^{-\nu/(n-m)} = (\tau_a\dot\gamma)^{-\nu/n} \quad (\varphi=\varphi_c). \qquad (13)$$

We will come back to this result later. A more extensive discussion of near-critical heterogeneous dynamics and the nature of the critical transition is given in Appendix B.

5. Origin of the heterogeneous dynamics

Based on evidence from experiments and simulations we have so far assumed that there are two diverging microscopic time scales, τ_η, for the single-particle mobility and $\tau_{\rm het} \gg \tau_\eta$ for the lifetime of the heterogeneous mobility pattern, the latter associated with a diverging correlation length ξ. Their dependence on the distance $|\Delta s|$ from criticality is given in our model by the power laws in (8), with critical exponents m, $n > m$, and ν, respectively. However, the origin of the growing heterogeneity in the dynamics upon approach of the critical point $s = s_c$ has not yet been discussed here. Fundamental aspects of this heterogeneous dynamics are still a subject of active research in the literature (see, e.g., Refs. [12,76–80]), both for glasses and jammed systems, and a detailed explanation is far beyond the scope of the present paper. For glasses at rest extensive simulations have been made from which both time scales could be recovered by analyzing the four-point dynamic correlation [81–84]. These simulations not only show the growing length and time scales but also their power-law interdependence.

Here we limit ourselves to a rather heuristic reasoning to understand the origin of the heterogeneity time scale and the associated exponent $n > m$. As is classically done for glasses [85], we consider a collectively rearranging region (CRR) of N particles and assume that they share one collective free volume v, of the order of a single-particle volume, to make rearrangements possible. We define a time τ such that all N particles will on average each have moved to a neighbor position. Associated with this, each particle will have experienced an individual free-volume change δv. For the statistics of this free-volume redistribution we now invoke a simple argument that is a variation on Mott's argument to explain creep by dislocation motion in metals [86] (see also Ref. [87]; Mott actually considers stress redistribution rather than free-volume redistribution). The fluctuations δv will scale as v/N and will be of either sign. If we assume them to be Gaussian, the average over a time $t = \tau$ of the CRR-summed fluctuation will vanish, $\langle\Sigma\delta v\rangle = 0$, while the average squared fluctuation will scale as $\langle(\Sigma\delta v)^2\rangle = \langle\Sigma(\delta v)^2\rangle \sim N(v/N)^2 \sim 1/N$. In the critical limit of diverging N this will also vanish and within the considered time τ nothing dramatic happens: the rearrangements will continue. However, the squared Gaussian fluctuations keep adding up linearly with time, so after a time $\tau' = N\tau$ we have $\langle\Sigma(\delta v)^2\rangle \sim v^2$. At this point the free-volume distribution has become such that there is a finite probability of arrest, so τ' is the lifetime τ_A of the mobile region. The rates $1/\tau$ and $1/\tau'$ refer to particles that are *a priori* taken as mobile, so $1/\tau_\eta = (1-s)/\tau$ and $1/\tau_{\rm het} = (1-s)/\tau'$. Accordingly, we have $\tau_{\rm het} = N\tau_\eta$. This argument shows that the large-scale fluctuating heterogeneity is a natural consequence of local fluctuations in the free volume and that in the critical limit in particular the ratio $\tau_{\rm het}/\tau_\eta$ diverges, whence $n > m$. If we characterize the CRR by its typical size ξ and (possibly fractal) dimension d we get with (8):

$$N = (\xi/\xi_a)^d = |1 - s/s_c|^{-\nu d} = |1 - s/s_c|^{m-n}. \qquad (14)$$

This gives us the relation $n = m + d\nu$ between the critical exponents. If we use this in (13) we see that the dependence of the size ξ of heterogeneous domains on the applied stress takes a very simple form at the critical concentration $\varphi = \varphi_c$ and by extension then also in the full critical shear-thinning region (the red region in Appendix B, Fig. 5): $\sigma\xi^d = \sigma_a\xi_a^d =$ constant. It expresses that the domain mass varies inversely proportional to the applied stress, the total energy supplied to a domain thus remaining constant. With the above exponent relation also the empirical yield-stress exponent $\Delta = \Gamma - M = n - m$ takes the very simple form $\Delta = d\nu$. We have derived this yield-stress exponent without considering the elastic phase explicitly, but only considering that the crossover should take place when $\sigma_{\rm visc} \approx \sigma_{\rm el} \approx \sigma_y$. It is intriguing to note that in Ref. [88] an exponent Δ of the same form is proposed for the elastic modulus near the critical gelation point of gels with entropic elasticity.

6. Power-law creep

So far, we only discussed the steady-state solution of Eq. (9). However, as discussed in the Introduction, transient creeping flow under nonsteady conditions is a generic feature of simple yield-stress fluids and many other materials. In fact, when the fluid is first exposed to a steady high stress and, subsequently, the stress is lowered to below the yield stress, a stress-independent viscosity develops that keeps increasing

as a power law in time [27,28]. In terms of our model this means that a system with $\varphi > \varphi_c$ is initially brought to a value $s(t)$ for the stagnant fraction that is well below s_c. In the rate equation (9) the dominant last term for particle arrest then rapidly brings s up near s_c again when the stress is lowered below σ_y, whereupon further arrest slows down. A time-dependent creep regime thus develops below σ_y in which $(1 - s/s_c)$ is already small but the arrest rate $1/\tau_A$ still dominates over the relaxation rate $1/\tau_R$. In this regime the time scales τ_A and τ_η have strongly increased and are well separated while the heterogeneity length scale ξ has correspondingly grown large. Just as in the steady state this heterogeneity scale will govern the dynamics and the same power laws apply, with the time entering via the nonconserved order parameter $s(t)$. So we get from (9):

$$ds/dt \approx (1 - s)/\tau_A \approx (1 - s_c)(1 - s/s_c)^n/\tau_a, \quad (|\Delta s| \ll s_c). \quad (15)$$

This is trivially integrated, with the result that for $t \gg \tau_a$ the distance from criticality $1 - s/s_c$ scales as an inverse power of time. Hence all power laws in this distance, or, equivalently, in ξ, also become power laws in time. In particular, we get for the viscosity of the creeping flow in the limit $t \gg \tau_a$ the functional form (5) proposed by Andrade [21] and verified for many different systems [13,22–31]: $\eta(t) \sim (t/\tau_a)^{m/(n-1)}$. So the Andrade creep exponent α can be expressed in terms of our exponents m and n as $\alpha = m/(n - 1)$. Note that the creeping-flow viscosity is indeed independent of the subcritical stress, due to the fact that far from steady state the stress-dependent relaxation term in the rate equation (9) could be ignored. Accordingly, the exponent α differs from the linear-response exponent $1 - \beta = m/n$ that would follow from the steady-state shear-thinning viscosity $\eta \sim \dot{\gamma}^{\beta-1}$.

IV. COMPARING THE MODEL TO EXPERIMENTAL DATA

A. Universal steady-state rheology

To judge the merits of the model we first note that it gives a microscopic basis for the scaling ansatz (6), which is accurately satisfied by the experimental data in Figs. 1–4. As is clear from Table I, the microscopic exponents $m = \Gamma - \Delta$ and $n = \Gamma$ or $m/n = 1 - \beta$ derived from the fits show little difference for the different experimental systems, notably for the two emulsions with strongly different particle interactions. Considering the numerical errors the exponents may well be universal to such 3D shear-driven dissipative systems, with typical values $m = 1.7$ and $n = 3.8$. The two microscopic time scales τ_a and τ_b that can be derived from our data in each case differ by many orders of magnitude: τ_b can be estimated from the crossover rate to shear thinning; on the other hand, the high-rate Newtonian regime IV above τ_a^{-1} is nowhere within reach, and, as a consequence, the asymptotic parameters τ_a and η_a cannot be determined from the data. Since the spatial heterogeneity has not been measured the third microscopic exponent ν cannot be determined either. In the literature a value around 0.7 has been suggested more than once [10,14,33,52]; together with our model prediction $\Delta = d\nu$ this would result in a realistic value $d = 3.0$. Furthermore, as shown already in Ref. [20] the soft emulsion gives within experimental accuracy a single power-law exponent $\Delta = B$ for the yield stress and shear modulus, respectively, and, consequently, a nonvanishing yield strain near φ_c.

B. Literature data

In the literature many other jamming systems have already been analyzed for their mechanical, rheological, or microstructural scaling laws, with a broad range of exponent values, partly at variance with the present data. For instance, in several papers [9,10,34–37] it is suggested that exponents should be independent of spatial dimension but sensitively dependent on the type of interparticle interaction; also the exponent Δ for the vanishing yield stress is claimed to be larger than the exponent B for the vanishing shear modulus, with a consequent vanishing of the yield strain near φ_c. These suggestions are supported by simulation data; however, it is not clear that the assumptions underlying these simulations would hold for all kinds of studied systems. Apart from the spatial dimension one should *a priori* distinguish, e.g., athermal versus Brownian systems and crossovers between the two [58–60,71,72], dry or wet systems with inertial effects and a subcritical Bagnold regime [34,35], and (quasi-)static simulated systems that are fully energy minimized [9,10]; in particular, the conclusions of interaction-dependent and dimension-independent exponents and of a vanishing yield strain are reached in the latter cases. Beyond the variety in studied systems is the problem of limited data range and accuracy, which may lead to practical curve fits rather than asymptotic scaling analysis, with correspondingly inaccurate exponents. In Appendix C we have collected from the literature measured or simulated exponent values for a broad range of systems (Table III), with similar systems grouped there together.

In the present discussion we compare in Table II our experimental data and model only with those systems that are clearly overdamped and athermal. Where possible and relevant we have added in bold italics additional exponent values that would result from applying our model to the published exponent values.

The flow-curve scaling demonstrated by Ref. [32] for an athermal soft suspension gives exponents very comparable to those in Figures 1–4: $\Gamma = 4.1$, $\Delta = 2.1$, so $m = 2.0$, $n = 4.1$. By contrast, the scaling around the jamming transition of overdamped simulated disks [33] gives $\Delta = 1.2$, $M = 1.65$, hence $\beta = 0.42$, and thus markedly different exponents $m = 1.65, n = 2.85$ in dimension 2; in a later study on the same 2D system by partly the same authors [38] a slightly lower value $\beta \approx 0.30$ is reported but still the exponents are argued to be universal for overdamped systems, so independent of details of particle interactions. The same authors also comment on the deviating results and conclusions of Ref. [36].

The simulated value $\nu = 0.73$ in Ref. [52] connects well with our equation $\Delta = d\nu$ and a yield-stress exponent $\Delta = 2.1$ as obtained here, while in the 2D simulations of Ref. [33] the values of Δ and d differ but the model prediction $\Delta = d\nu$ is still satisfied. In the 2D study of Ref. [33] there is also an accurately satisfied scaling ansatz for ξ versus σ, with a consequential relation $\xi \sim \sigma^{-\nu/\Delta}$ in the critical regime; with our identification $\Delta = n - m$ this relation is the same as (13).

TABLE II. Experimental, simulated or predicted scaling exponents for shear-driven overdamped systems. In bold italics additional exponents are given that result from applying our model to the published exponent values (*second entry: lowest concentration omitted).

Ref	System		Exponents of flow-curve scaling				Exponents of microscopic time- and lengthscales			
			Yield stress	Cross-over rate	Shear thinning	Krieger-Dougherty	Single-particle mobility	Cooperative dynamics	Correlation length	
			Δ	Γ	β	M	m	n	ν below φ_c	above φ_c
This work	model prediction	all d	$n - m$	n	$1 - m/n$	m			$(n - m)/d$	$\xi \sim L$ at $\sigma = \sigma_y$
	soft emulsion ~ 3.2μ (data from [20])	$d = 3$	2.13	3.84	0.55	1.71				
					0.55	***1.71***	***1.71***	***3.84***	***0.71***	
	rigid emulsion		2.04	3.80	0.54					
					0.54	***1.76***	***1.76***	***3.80***	***0.68***	
	foam (data from [62])		2.21	3.75	0.57					
					0.59	***1.54***	***1.54***	***3.75***	***0.74***	
	Carbopol gel				0.48/0.55 *					
							m/n = 0.52/0.45*			
[32]	NiPA~ 1μ		2.1	4.1	0.48					
					0.51	***2.0***	***2.0***	***4.1***	***0.7***	
[52]	overdamped simulation harmonic interaction							3.3	0.73	
			2.1	***3.3***	***0.64***	***1.2***	***1.2***			
[55]					0.64				$m/n = 0.27, \nu/n = 0.23$	
					0.69-0.73				***m/n = 0.36***	
[64]	overdamped simulation unspecified interaction					1.7				
[33]	overdamped simulation harmonic interaction	$d = 2$	1.2			1.65			0.6	
				2.85	***0.42***		***1.65***	***2.85***	***0.6***	
[38]			1.08		0.30				$\nu = 0.18n$ at $\varphi = \varphi_c$	
				3.0-3.6	***0.36***	***1.9-2.5***	***1.9-2.5***	***3.0-3.6***	***0.54-0.65***	
[53]									0.9	$\xi \sim L$ at $\sigma = \sigma_y$
[54]			1.05							$\xi \sim L$ at $\sigma = \sigma_y$
[36]					0.5					
	overdamped model harmonic interaction		3/2		1/2					
				3		***3/2***	***3/2***	***3***	***1/2***	

In the related study of Ref. [38] ξ has been measured near φ_c as a power of $\dot{\gamma}^{-1}$, with the result $\nu/\Gamma = \nu/n = 1/5.6$; within the reported numerical accuracy for ν this is consistent with the exponents of Ref. [33]. In the 3D simulation of Ref. [55] ξ has been measured close to φ_c as a power of $\dot{\gamma}^{-1}$, with an exponent 0.23; for our emulsions, assuming $\nu = 0.7$, Eq. (13) would give an exponent 0.18. The model assumption that for concentrations above φ_c the correlation length diverges on approach of the yield stress, i.e., that the scale of the heterogeneous dynamics becomes of the system size L in the quasistatic limit, has been confirmed in the simulations of Refs. [53,54,68].

The divergence of the microscopic time scales τ_η and $\tau_{\rm het}$ has been little studied in a direct and quantitative manner. In the simulations by Ref. [52] of a 3D overdamped system a power-law divergence of the heterogeneity time scale was indeed found, with an exponent $n = 3.3$, somewhat below our value 3.8 for Γ. The simulations in Ref. [55] of the velocity autocorrelation and the spatial correlations imply a ratio of exponents $m/n = 0.27$, so there is, indeed, a strong separation of the two time scales, although this actual value is below our ratio of ca. 0.45. The samples of Ref. [32] that showed much similarity to ours in the scaling of flow curves have also been investigated for their microscopic and heterogeneous dynamics [56]. Data covering the shear-thinning regime as well as the plateau regime show a single power-law relation between the mass of cooperative regions and the single-particle relaxation time, strengthening the concept of one dominant variable close to the critical transition. Using our equality $\tau_{\rm het} = N\tau_\eta$ these results translate into a fairly low Herschel-Bulkley exponent $\beta = 1 - m/n = 0.24$, much lower also than earlier reported [32] from flow-curve scaling. The authors also report a very accurate scaling of the mass and relaxation time with the product of variables $\dot{\gamma}|\Delta\varphi|^4$ that cannot be explained by our model; we expect the dependence on these two variables to differ. The origin of the discrepancy remains unclear, but we note that in the measurements a significant stress and rate gradient was present over the larger cooperative domains, thus making the relation between the domain size and a single value for the order parameter s meaningless.

In sum, Table II shows that there is often good agreement when comparing the present theory and emulsion data with the steady-state rheology of other overdamped and athermal literature systems, especially as regards the existence of the scaling laws. The exponent values in the table support the idea that the scaling around the jamming transition is universal for such systems, being only dependent on the spatial dimension but not on details of the interaction. The larger collection of data in Appendix C, Table III reveals much more variety in the exponent values, partly due to numerical inaccuracy but, more importantly, as a result of different underlying mechanisms or simulation assumptions.

In this paper the main focus is on steady-state rheology. However, one of the key issues in the behavior of yield-stress fluids is the creep behavior, which as shown above can also be covered by the model. It was demonstrated recently [27,28] that creep was the reason for sometimes wrongly interpreted "liquidlike" behavior of yield-stress materials below σ_y; in fact the creep is then so slow that a steady state is not reached within experimental time scales and so the apparent "viscosity" keeps on increasing in time, following the Andrade law (5). From the exponents m and n that characterize the steady-state rheology, our model predicts the exponent for the transient Andrade creep as $\alpha = m/(n-1)$. This prediction was tested on the soft emulsion with volume fraction $\varphi = 0.66$, just above φ_c [20]. The steady-state data predict $\alpha = 0.60$, whereas the creep data accurately satisfy $\alpha = 0.6$, in close correspondence also with many observations in the literature.

V. CONCLUSIONS

We have determined and numerically analyzed the experimental steady-state flow behavior of four different yield-stress systems: two emulsions, with mobile and rigid particle surfaces, respectively, a 3D foam, and a Carbopol gel. While the particle interactions of all four overdamped systems can be assumed to be rather different, their rheology near and across the critical jamming transition was found to obey universality: By appropriate scaling with the distance to jamming all systems allowed a data collapse onto supercritical Herschel-Bulkley and (where accessible) subcritical Cross master curves that meet at critical shear thinning; moreover, the sets of independent scaling exponents proved the same within numerical error for the different systems.

To rationalize such critical scaling we have presented a simple microscopic two-state theory in which the steady state is a balance between stagnant and fluidized particles and where the stagnant fraction is the internal order parameter that is driven to criticality. Heterogeneous microscopic dynamics is at the heart of this theory and the two empirical scaling exponents could be related to exponents for two diverging time scales: for the single-particle fluidity and for the lifetime of the fluctuating heterogeneous domains. A third microscopic exponent describes the critical divergence of the heterogeneity length scale, not only near the jamming point but along the full yield-stress line. A heuristic argument based on fluctuations in the local free volume explains the origin of the heterogeneous dynamics and is able to give a scaling relation among the exponents. The theory also predicts power-law creep.

The experimentally determined exponents and the predictions of the microscopic model have been compared with a large set of literature data, giving additional support both for the model and for the assumed universality among overdamped frictionless yield-stress systems of the same dimension. For other systems exponents clearly differ.

ACKNOWLEDGMENTS

We thank Arnaud Saint Jalmes for helpful discussions on the data of Marze and Martin van Hecke and Brian Tighe for interesting discussions about the universality (or not) of the exponents.

APPENDIX A: DERIVATION OF THE STEADY-STATE BEHAVIOR

The mathematical problem to solve in the different regimes of concentration and flow can be summarized in one line as:

$$s[(\tau_a/\tau_b) f_\pm(\sigma/\sigma_y) + \tau_a\dot{\gamma}] = (1 - s/s_c)^n = (\eta_a/\eta)^{n/m}, \tag{A1}$$

with $\tau_b/\tau_a \gg 1$, with $n > m$ and with $f_\pm(x)$ given by:

$$f_+(x) = (x-1)^p, \quad x > 1 \ (\varphi > \varphi_c);$$
$$f_+(x) \equiv 0, \ x < 1 \ (\varphi > \varphi_c), \tag{A2}$$

$$f_-(x) = 1 \ (\varphi < \varphi_c). \tag{A3}$$

Let us first consider the solution of (A1) in the limit $s \downarrow 0$. In this limit the viscosity becomes Newtonian, both above and below the critical concentration: $\eta = \eta_a$ and $\sigma = \eta_a\dot\gamma$. However, it corresponds to very high stresses and rates that may often not be accessible experimentally: $\dot\gamma \gg 1/\tau_a$. The stagnant fraction s vanishes as $(\tau_a\dot\gamma)^{-1}$.

With decreasing stress and rate the viscosity increases far above η_a and the solids fraction approaches the critical value s_c. When the second term at the left-hand side of (A1) (i.e., collective flow) still dominates the relaxation, the viscosity and viscous stress are seen to become power law in the rate: $\eta = \eta_a(\tau_a\dot\gamma)^{-m/n}$ and hence $= (\eta_a/\tau_a)(\tau_a\dot\gamma)^{1-m/n}$, $\eta = \eta_a(\eta_a/\tau_a\sigma)^{m/(n-m)}$ (here we suppress an overall factor $s \approx s_c$, which is of order unity). Also this power-law shear-thinning rheology applies to both sides of φ_c, making the critical transition continuous. As is clear from (A1) it corresponds to rates $1/\tau_b \ll \dot\gamma \ll 1/\tau_a$. The small distance Δs from criticality follows directly from the viscosity as $|\Delta s/s_c| = (\tau_a\dot\gamma)^{-1/n} = (\eta_a/\tau_a\sigma)^{-1/(n-m)}$.

Upon further increase of the stagnant fraction and viscosity the two terms at the left-hand side of (A1) become of equal order and a crossover happens to a regime where the collective flow is no longer dominant. If we assume that the elastic stress is of the order of the yield stress, this crossover should correspond with $\Delta\sigma \cong \sigma_y$. Accordingly, $f(\sigma/\sigma_y)$ will be of order unity and the crossover rate of the order $1/\tau_b$, both above and below φ_c. Inserting these crossover conditions in the expressions of the shear-thinning regime we get the yield stress as $\sigma_y = (\eta_a/\tau_a)(\tau_b/\tau_a)^{-(1-m/n)}$. Note that this yield stress has been found from the crossover conditions, without modeling the response in the static elastic regime.

For lower stresses or rates the first term at the left-hand side of (A1) becomes dominant and the solution splits, depending on the sign of $\Delta\varphi$. Above the jamming concentration we use (A2) and then get for $\Delta\sigma \ll \sigma_y$ or, equivalently, $\dot\gamma \ll 1/\tau_b$ the solution $\eta = \eta_a(\tau_b/\tau_a)^{m/n}(\sigma_y/\Delta\sigma)^{pm/n}$. Inserting the above expression for σ_y and taking $\Delta\sigma$ equal to the viscous stress $\eta\dot\gamma$ we then find the total stress in this plateau regime as $\sigma = \sigma_y[1 + (\tau_b\dot\gamma)^{1/(1+pm/n)}]$. Again the small distance Δs from criticality follows directly from the viscosity via (A1). The expressions in this regime still contain the exponent p that characterizes the stress-dependent escape rate. In principle p may be left as a separate parameter, dependent on details of the jamming mechanism. Olsson and Teitel [89] have analyzed the rheology of soft particles near the athermal jamming transition by mapping onto a hard-core system and deriving from it that the Herschel-Bulkley exponent would equal the inverse of the Krieger-Dougherty exponent: $\beta = 1 - m/n \ = 1/m$, which leaves one independent exponent only. However, their derivation is based on an expansion in powers of $\dot\gamma$ at finite and positive $\Delta\sigma$, i.e., near the quasistatic limit in the plateau regime where elastic energies still dominate; with the expression for the rate-dependent stress in this regime the argument of Ref. [89] actually gives $p = n(1 - 1/m)$, so still two independent exponents. On a par with the Herschel-Bulkley equation we pragmatically make here the simplifying assumption that the minor excess viscous stress of the plateau regime has the same rate dependence as the much larger viscous stress of the shear-thinning regime. This is realized by the practical choice $p = (1 - m/n)^{-1}$, which makes the viscous stresses in the two regimes fully identical.

Below the critical concentration and again for $\dot\gamma \ll 1/\tau_b$ we insert (A3); then normal Newtonian rheology is found, with a very high viscosity: $\eta_N = \eta_a(\tau_b/\tau_a)^{m/n}$.

APPENDIX B: NEAR-CRITICAL HETEROGENEOUS DYNAMICS AND THE NATURE OF THE CRITICAL TRANSITION

With the mapping of the mathematical solution onto the empirical flow equations our model covers the full empirical rheology that is contained in the scaling ansatz (6) for the solid-fluid transition. This allows us to interpret the transition in terms of the microscopic order parameter, i.e., the instantaneous stagnant fraction s and the associated diverging heterogeneity length scale $\xi(s)$. To do so, we consider in Fig. 5 the 3D diagram with the schematic flow surface $\sigma = \sigma(\varphi,\dot\gamma)$.

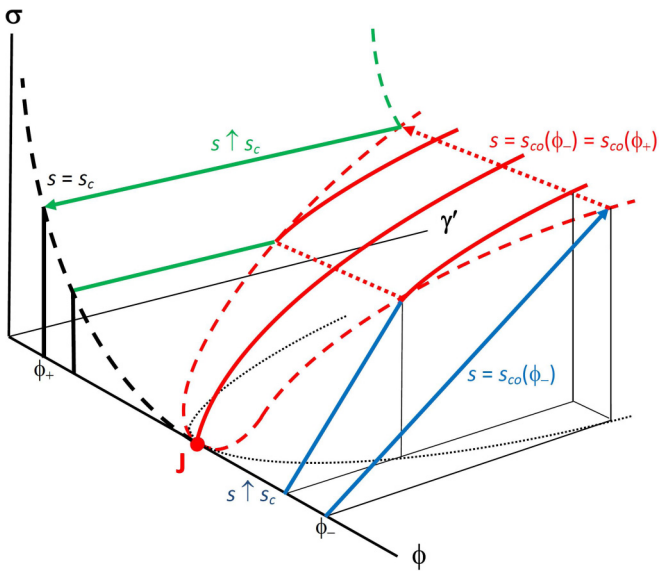

FIG. 5. (Color online) Three-dimensional diagram of concentration φ, stress σ, and rate $\dot\gamma$. The steady-state flow surface $\sigma = \sigma(\varphi,\dot\gamma)$ is formed by the blue, red, and green areas (from bottom to top), representing low-rate Newtonian flow, critical shear thinning, and supercritical plateau stress, respectively. The crossover borders between these areas are only sharp in the jamming point J, where they all meet. The evolution through the flow surface of the microscopic order parameter s, the stagnant fraction, is indicated. The black area of elastic response is bounded by the yield-stress line $\sigma_y(\varphi)$, where s reaches its critical value s_c.

TABLE III. Experimental, simulated, or predicted scaling exponents from a broad range of rheological and microscopic data. In the third column aspects are indicated in which systems essentially differ from the yield-stress fluids studied in this paper.

Ref	System		Exponents of flow-curve scaling			Linear-response exponents		Exponents of microscopic time- and lengthscales			
			Yield stress	Cross-over rate	Shear thinning	Viscosity	Shear modulus	Single-particle mobility	Cooperative dynamics	Correlation length	
			Δ	Γ	β	M	B	m	n	ν below φ_c	above φ_c
This work	model prediction	all d	$n - m$	n	$1 - m/n$	m				$(n - m)/d$	$\xi \sim L$ at $\sigma = \sigma_y$
	soft emulsion $\sim 3.2\,\mu$ (data from [20])	$d = 3$	2.13	3.84	0.55	1.71	2.1				
	rigid emulsion		2.04	3.80	0.54						
	foam (data from [62])		2.21	3.75	0.57						
	Carbopol gel				0.48-0.55						
[20]	NiPA $\sim 1\,\mu$	$d = 3$	2.1	4.1	0.48						
[52]	overdamped simulation harmonic interaction								3.3	0.73	
[55]					0.64				$m/n = 0.27$, $\nu/n = 0.23$		
[64]	overdamped simulation unspecified interaction					1.7					
[56]	NiPA ~ 0.6-$1.0\,\mu$	$d = 3$ data not fully athermal?							$N_{CRR} \sim \tau_\eta^{0.31}$		
[57]	NiPA ~ 0.6-$0.8\,\mu$									0.5	
[72]	NiPA $\sim 0.6\,\mu$		2.6	5.0-5.6	0.52-0.46		1.0				
[45]	NiPA $\sim 0.1\,\mu$					2.25					$\xi \sim L$ at $\sigma = 0$, $\varphi = \varphi_c$
[59]	range of literature data	$d = 3$ combined fit of glass and jamming singularities	1.0-2.0		0.4-0.6	2.0					
[71]	emulsion ~ 0.5-$1.1\,\mu$		1.2				0.82				
[58]	overdamped simulation harmonic interaction		1.2		0.4	2.0					

TABLE III. (*Continued.*)

Ref	System		Exponents of flow-curve scaling			Linear-response exponents		Exponents of microscopic time- and lengthscales			
			Yield stress	Cross-over rate	Shear thinning	Viscosity	Shear modulus	Single-particle mobility	Cooperative dynamics	Correlation length	
			Δ	Γ	β	M	B	m	n	ν below φ_c	above φ_c
[33]	overdamped simulation harmonic interaction	$d = 2$	1.2			1.65				0.6	
[38]			1.08		0.30					$\nu/n = 0.18$ at $\varphi = \varphi_c$	
[53]										0.9	$\xi \sim L$ at $\sigma = \sigma_y$
[54]			1.05								$\xi \sim L$ at $\sigma = \sigma_y$
[36]	overdamped model harmonic interaction		3/2		0.5 1/2		1/2				
[34] [35]	inertial model harmonic interaction	all d	1	5/2	Δ/Γ	$2\Gamma - \Delta$					
	inertial model hertzian interaction		3/2	11/4							
	inertial simulation harmonic interaction	$d = 2$-4	1.0	2.5	0.4	4.0					
[64]	inertial simulation harmonic interaction	$d = 3$	1.2	1.9							
	inertial simulation hertzian interaction		1.8	2.4							
[51]	air-driven beads	$d = 2$								1.7	
[50]	air-fluidized beads								1.03	0.72	
[10]	quasistatic simulation harmonic interaction	$d = 2,3$					0.5				0.71 at $\sigma = 0$
	quasistatic simulation hertzian interaction						1.0				0.71 at $\sigma = 0$

The regimes I–III are shown in blue, green, and red, respectively; the regime of only elastic response (solid black lines), which is not addressed in our model, is the $\sigma - \varphi$ plane bounded by the dashed black yield-stress curve $\sigma_y(\varphi)$. As is clear already from the scaling ansatz the critical jamming point J at $\varphi = \varphi_c$ widens with increasing rate into a tongue-shaped area (red) bounded by the crossover rate; the latter grows on both sides of φ_c as a power law with $|\Delta\varphi|$ (dotted line in the bottom plane). In this area of power-law shear thinning (regime III, with the solid red lines representing the flow curves) the subcritical Newtonian phase (regime I, blue) and the supercritical nearly stagnant plateau phase (regime II, green) have become indistinguishable. Note that the figure is only schematic and that in reality the blue and green flow curves (solid lines) are not fully straight or flat and the red area may be somewhat tilted and its boundaries (dashed) are not sharp.

In this figure the growth of the stagnant fraction can now be followed by starting at a concentration $\varphi_- < \varphi_c$ in the low-rate regime. Since the flow is here Newtonian, s cannot vary with σ or $\dot\gamma$ until, along the blue arrow (increasing rate at constant concentration), the critical regime is hit. Within that regime all states are indistinguishable along the φ direction, i.e., along the dotted red arrow that brings us at the concentration $\varphi_+ > \varphi_c$ where the plateau regime is entered; so, again, s has not varied. Only from that point will s raise when the green arrow (decreasing rate at constant concentration) is followed, until it reaches its maximum value s_c at the yield-stress curve. When the starting point φ_- (and hence also φ_+) is chosen closer to J, the starting value of s will be higher, ultimately reaching s_c in the jamming point. The correlation length ξ, and the fluidity and heterogeneity time scales τ_η and $\tau_{\rm het}$ and their ratio $\tau_{\rm het}/\tau_\eta$, diverge with decreasing $|\Delta s|$; so they are all infinite along the full yield-stress curve.

A general conclusion from the above is that although in the quasistatic limit the Newtonian fluid at φ_- and the yield-stress solid at φ_+ obviously differ, a continuous path between them exists via the power-law shear-thinning regime where the two phases become indistinguishable. A qualitative analogy with a second-order phase transition presents itself, but a sharp transition only happens in the limit where the two crossover lines meet, i.e., at $\varphi = \varphi_c$ (see Fig. 5). In the jamming point $J(\varphi = \varphi_c, \sigma = 0)$ the correlation length ξ is infinite, as in a classical second-order critical point; at the critical concentration a finite external stress σ drives the system away from the singularity in a power-law fashion, according to Eq. (13). However, the diagram is clearly more complicated than for classical phase transitions. The divergence of the correlation length is continued from the point J onward along the full yield-stress line, which marks the quasistatic limit at which a sharp transition to the jammed solid phase happens for $\varphi > \varphi_c$. The present paper does not address the jammed phase itself. Theories of this phase with $\varphi > \varphi_c$ often focus on its linear-elastic behavior and consider another characteristic length $\tilde\xi$, which diverges when J is approached by decreasing φ to φ_c along the equilibrium line $\sigma = \dot\gamma = 0$; that length $\tilde\xi$ measures the domain size beyond which the system is overcoordinated and behaves as an ordinary solid [11,65,66,69]. Moving away from this equilibrium line by elastic deformation, along the upward solid black lines in Fig. 5, destabilizes the solid phase and will increase the size $\tilde\xi$ of isostatic domains. Ultimately the elastic stress drives the solid to the yield-stress line; here $\tilde\xi$ diverges and thus naturally meets the divergent correlation length ξ of the fluidized phase.

APPENDIX C: TABLE OF LITERATURE DATA

In Table III we have collected experimental or simulated exponent values for a broad range of systems, with similar systems grouped together to ease comparison. In spite of the variety in all these values some observations can still be made in addition to those already discussed in the main text for athermal overdamped systems.

The table includes additional overdamped experimental systems [45,56,57,72] which are supposed to be influenced, at least in part, by thermal effects.

The exponent values from flow-curve scaling for inertial systems with Bagnold scaling below φ_c, both obtained theoretically and by simulation [34,35], clearly differ from those of the overdamped systems and turn out to be interaction dependent and dimension independent. In Ref. [64] the flow-curve scaling for a simulated inertial system gave exponents that somewhat differ from Refs. [34,35] but are still clearly interaction dependent and differ from ours. Note that athermal systems with weak viscous damping may also crossover to an inertia-dominated shear-thickening Bagnold regime very close to φ_c [90]. Such systems should be modeled by particle exchange between three rather than two microscopic states. However, extension from the present model is not straightforward since the inertial dynamics introduces important new mechanisms beyond what is covered in the rate equation (9) with (8) and (10).

As is clear also from Table III, there are broad indications for heterogeneous dynamics as also assumed in our model, with a diverging associated length scale ξ when φ_c is approached from below [10,45,49,50,52,53,57]. Note that the definition of ξ may vary here; in particular, both two-point and four-point correlations have been considered. Often there is evidence for a power-law divergence in $|\Delta\varphi|$, with the associated exponent ν generally below unity. Interestingly, a correlation-length exponent around 0.7 is obtained both in overdamped and inertial 2D and 3D systems.

Heterogeneous dynamics is also frequently observed in liquids approaching the thermal glass transition, with a growing correlation length and a separation of two time scales; power laws are often assumed. However, as pointed out [58–60,72], the microscopic dynamics, the critical concentration, and the rheology scaling then differ. Combined fits can even be made of the glass and jamming singularities [58–59,71], although this may influence an accurate determination of the separate rheological exponents. For glasses at rest (not included in the table) power-law relations between a heterogeneity length scale and well-separated microscopic time scales have been accurately established by simulations, with implied exponent ratios $n/m = 1.5$ and $n/\nu = 5.4$ for soft spheres [81,82,84] and $n/m = 1.75$ for 2D colloids [83].

[1] R. G. Larson, *The Structure and Rheology of Complex Fluids* (Oxford University Press, New York, 1999).
[2] M. M. Denn and D. Bonn, Rheol. Acta **50**, 307 (2011).
[3] D. Bonn, J. Paredes, M. M. Denn, L. Berthier, T. Divoux, and S. Manneville, arXiv:1502.05281 (2015).
[4] A. Liu and S. R. Nagel, Nature **396**, 21 (1998).
[5] A. J. Liu and S. R. Nagel (eds.), *Jamming and Rheology* (CRC Press, Boca Raton, FL, 2001).
[6] V. Trappe, V. Prasad, L. Cipelletti, P. N. Segre, and D. A. Weitz, Nature **411**, 772 (2001).
[7] F. Da Cruz, F. Chevoir, D. Bonn, and P. Coussot, Phys. Rev. E **66**, 051305 (2002).
[8] D. Bonn, P. Coussot, H. T. Huynh, F. Bertrand, and G. Debregeas, Europhys. Lett. **59**, 786 (2002).
[9] C. S. O'Hern, S. A. Langer, A. J. Liu, and S. R. Nagel, Phys. Rev. Lett. **88**, 075507 (2002).
[10] C. S. O'Hern, L. E. Silbert, A. J. Liu, and S. R. Nagel, Phys. Rev. E **68**, 011306 (2003).
[11] A. J. Liu and S. R. Nagel, Annu. Rev. Condens. Matter Phys. **1**, 347 (2010).
[12] L. Berthier, G. Biroli, J.-P. Bouchaud, L. Cipelletti, and W. van Saarloos (eds.), *Dynamical Heterogeneities in Glasses, Colloids, and Granular Materials* (Oxford University Press, New York, 2011).
[13] M.-Carmen Miguel, A. Vespignani, M. Zaiser, and S. Zapperi, Phys. Rev. Lett. **89**, 165501 (2002).
[14] J. A. Drocco, M. B. Hastings, C. J. Olson Reichhardt, and C. Reichhardt, Phys. Rev. Lett. **95**, 088001 (2005).
[15] G. Biroli, Nat. Phys. **3**, 222 (2007).
[16] W. H. Herschel and R. Bulkley, Kolloid Z. **39**, 291 (1926).
[17] M. Cross, J. Colloid Sci. **20**, 417 (1965).
[18] I. M. Krieger and T. J. Dougherty, J. Rheol. **3**, 137 (1959).
[19] B. P. Tighe, Phys. Rev. Lett. **107**, 158303 (2011).
[20] J. Paredes, M. A. J. Michels, and D. Bonn, Phys. Rev. Lett. **111**, 015701 (2013).
[21] E. N. da Costa Andrade, Proc. Roy. Soc. A **84**, 1 (1910).
[22] M.-C. Miguel, P. Moretti, M. Zaiser, and S. Zapperi, Mater. Sci. Eng. A **400–401**, 191 (2005).
[23] M.-C. Miguel, L. Laurson, and M. J. Alava, Eur. Phys. J. B **64**, 443 (2008).
[24] L. Laurson, M.-Carmen Miguel, and M. J. Alava, Phys. Rev. Lett. **105**, 015501 (2010).
[25] M. Siebenbürger, M. Ballauff, and T. Voigtmann, Phys. Rev. Lett. **108**, 255701 (2012).
[26] G. B. McKenna, J. Phys.: Condens. Matter **15**, S737 (2003).
[27] P. C. F. Møller, A. Fall, and D. Bonn, Europhys. Lett. **87**, 38004 (2009).
[28] P. Møller, A. Fall, V. Chikkadi, D. Derks, and D. Bonn, Phil. Trans. Roy. Soc. A **367**, 5139 (2009).
[29] J. W. Dudley, M. T. Myers, R. D. Shew, and M. M. Arasteh, SPE Reserv. Eval. Eng. **1**, 430 (1998).
[30] J. Rosti, J. Koivisto, L. Laurson, and M. J. Alava, Phys. Rev. Lett. **105**, 100601 (2010).
[31] C. D. Agosti, K. M. Bell, D. J. Plazek, J. Larson, J. D. Kang, L. G. Gilbertson, and P. Smolinski, Biorheology **47**, 143 (2010).
[32] K. N. Nordstrom, E. Verneuil, P. E. Arriata, A. Basu, Z. Zhang, A. G. Yodh, J. P. Gollub, and D. J. Durian, Phys. Rev. Lett. **105**, 175701 (2010).
[33] P. Olsson and S. Teitel, Phys. Rev. Lett. **99**, 178001 (2007).
[34] M. Otsuki and H. Hayakawa, Prog. Theor. Phys. **121**, 647 (2009).
[35] M. Otsuki and H. Hayakawa, Phys. Rev. E **80**, 011308 (2009).
[36] B. P. Tighe, E. Woldhuis, J. J. C. Remmers, W. van Saarloos, M. van Hecke, Phys. Rev. Lett. **105**, 088303 (2010).
[37] G. Katgert, B. P. Tighe, and M. van Hecke, Soft Matter **9**, 9739 (2013).
[38] D. Vågberg, P. Olsson, and S. Teitel, Phys. Rev. Lett. **113**, 148002 (2014).
[39] M. D. Ediger, Annu. Rev. Phys. Chem. **51**, 99 (2000).
[40] R. Richert, J. Phys.: Condens. Matter **14**, R703 (2002).
[41] E. Aharonov, E. Bouchbinder, H. G. E. Hentschel, V. Ilyin, N. Makedonska, I. Procaccia, and N. Schupper, Europhys. Lett. **77**, 56002 (2007).
[42] R. A. Riggleman, H.-N. Lee, M. D. Ediger, and J. J. de Pablo, Phys. Rev. Lett. **99**, 215501 (2007).
[43] R. A. Riggleman, K. S. Schweizer, and J. J. de Pablo, Macromolecules **41**, 4969 (2008).
[44] H.-N. Lee, K. Paeng, S. F. Swallen, and M. D. Ediger, Science **323**, 231 (2009).
[45] D. A. Sessoms, I. Bischofsberger, L. Cipelletti, and V. Trappe, Phil. Trans. Roy. Soc. A **367**, 5013 (2009).
[46] R. A. Riggleman, H.-N. Lee, M. D. Ediger, and J. J. de Pablo, Soft Matter **6**, 287 (2010).
[47] S. Maccarone, G. Brambilla, O. Pravaz, A. Duri, M. Ciccotti, J.-M. Fromental, E. Pashkovski, A. Lips, D. Sessoms, V. Trappe, and L. Cipelletti, Soft Matter **6**, 5514 (2010).
[48] H.-N. Lee and M. D. Ediger, Macromolecules **43**, 5863 (2010).
[49] A. S. Keys, A. R. Abate, S. C. Glotzer, and D. J. Durian, Nat. Phys. **3**, 260 (2007).
[50] A. R. Abate and D. J. Durian, Phys. Rev. E **76**, 021306 (2007).
[51] F. Lechenault, O. Dauchot, G. Biroli, and J. P. Bouchaud, Europhys. Lett. **83**, 46003 (2008).
[52] T. Hatano, Phys. Rev. E **79**, 050301(R) (2009).
[53] C. Heussinger, L. Berthier, and J.-L. Barrat, Europhys. Lett. **90**, 20005 (2010).
[54] C. Heussinger, P. Chaudhuri, and J.-L. Barrat, Soft Matter **6**, 3050 (2010).
[55] T. Hatano, J. Phys. Conf. Ser. **319**, 012011 (2011).
[56] K. N. Nordstrom, J. P. Gollub, and D. J. Durian, Phys. Rev. E **84**, 021403 (2011).
[57] Y. Rahmani, K. van der Vaart, B. van Dam, Z. Hu, V. Chikkadi, and P. Schall, Soft Matter **8**, 4264 (2012).
[58] A. Ikeda, L. Berthier, and P. Sollich, Phys. Rev. Lett. **109**, 018301 (2012).
[59] A. Ikeda, L. Berthier, and P. Sollich, Soft Matter **9**, 7669 (2013).
[60] P. Olsson and S. Teitel, Phys. Rev. E **88**, 010301(R) (2013).
[61] S. A. Koehler, S. Hilgenfeldt, E. R. Weeks, and H. A. Stone, Phys. Rev. E **66**, 040601(R) (2002).
[62] S. Marze, D. Langevin, and A. Saint-Jalmes, J. Rheol. **52**, 1091 (2008).
[63] J. F. Paredes Rojas, Ph.D. thesis, University of Amsterdam, 2013.
[64] T. Hatano, J. Phys. Soc. Jpn. **77**, 123002 (2008).
[65] M. Wyart, S. R. Nagel, and T. A. Witten, Europhys. Lett. **72**, 486 (2005).
[66] W. G. Ellenbroek, E. Somfai, M. van Hecke, and W. van Saarloos, Phys. Rev. Lett. **97**, 258001 (2006).
[67] C. Heussinger and J.-L. Barrat, Phys. Rev. Lett. **102**, 218303 (2009).
[68] K. Martens, L. Bocquet, and J.-L. Barrat, Phys. Rev. Lett. **106**, 156001 (2011).

[69] C. P. Goodrich, W. G. Ellenbroek, and A. J. Liu, Soft Matter **9**, 10993 (2013).
[70] H. Eyring, J. Chem. Phys. **4**, 283 (1936).
[71] F. Scheffold, F. Cardinaux, and T. G. Mason, J. Phys.: Condens. Matter **25**, 502101 (2013).
[72] A. Basu, Y. Xu, T. Still, P. E. Arriata, Z. Zhang, K. N. Nordstrom, J. M. Rieser, J. P. Gollub, D. J. Durian, and A. G. Yodh, Soft Matter **10**, 3027 (2014).
[73] M. Grob, C. Heussinger, and A. Zippelius, Phys. Rev. E **89**, 050201 (2014).
[74] E. Irani, P. Chaudhuri, and C. Heussinger, Phys. Rev. Lett. **112**, 188303 (2014).
[75] H. M. Wyss, K. Miyazaki, J. Mattsson, Z. Hu, D. R. Reichman, and D. A. Weitz, Phys. Rev. Lett. **98**, 238303 (2007).
[76] G. Biroli, J.-P. Bouchaud, K. Miyazaki, and D. R. Reichman, Phys. Rev. Lett. **97**, 195701 (2006).
[77] D. Hajnal and M. Fuchs, Eur. Phys. J. E **28**, 125 (2009).
[78] E. Flenner and G. Szamel, Phys. Rev. Lett. **105**, 217801 (2010).
[79] C. Fusco, T. Albaret, and A. Tanguy, Eur. Phys. J. E **37**, 43 (2014).
[80] J. Lin, E. Lerner, A. Rosso, and M. Wyart, Proc. Natl. Acad. Sci. USA **111**, 14382 (2014).
[81] K. Kim and S. Saito, Phys. Rev. E **79**, 060501(R) (2009).
[82] K. Kim and S. Saito, J. Chem. Phys. **133**, 044511 (2010).
[83] H. Tanaka, T. Kawasaki, H. Shintani, and K. Watanabe, Nat. Mater. **9**, 324 (2010).
[84] K. Kim and S. Saito, J. Chem. Phys. **138**, 12A506 (2013).
[85] G. Adam and J. H. Gibbs, J. Chem. Phys. **43**, 139 (1965).
[86] N. F. Mott, Philos. Mag. **44**, 742 (1953).
[87] F. Louchet and P. Duval, Int. J. Mater. Res. **100**, 1433 (2009).
[88] X. Xing, S. Mukhopadhyay, and P. M. Goldbart, Phys. Rev. Lett. **93**, 225701 (2004).
[89] P. Olsson and S. Teitel, Phys. Rev. Lett. **109**, 108001 (2012).
[90] A. Fall, A. Lemaître, F. Bertrand, D. Bonn, and G. Ovarlez, Phys. Rev. Lett. **105**, 268303 (2010).